

Article

Study on the Skeleton Mechanism of Second-Generation Biofuels Derived from Platform Molecules

Weiwei Fan ^{1,*} , Aichun Du ², Gang Liu ¹, Qing Liu ¹ and Yuan Gao ¹¹ School of Vehicle and Traffic Engineering, Henan Institute of Technology, Xinxiang 453003, China² Department of Machinery and Electronics Engineering, Hami Polytechnic University, Hami 839000, China

* Correspondence: fww@hait.edu.cn; Tel.: +86-373-3691053

Abstract: This paper focuses on the combustion mechanism of furan-based fuels synthesized from lignocellulose. The fuel is a binary alternative fuel consisting of 2-methylfuran and 2,5-dimethylfuran derived from furfural. The key reactions affecting the combustion mechanism of this fuel were identified via path analysis, and the initial reaction kinetic mechanism was constructed using a decoupling methodology. Then, a genetic algorithm was used to optimize the initial mechanism. The final skeleton mechanism consisted of 67 species and 228 reactions. By comparing experimental data on ignition delay, component concentration, and laminar flame velocity under a wide range of conditions over various fundamental reactors, it was shown that the mechanism has the ability to predict the combustion process of this fuel well.

Keywords: skeleton mechanism; genetic algorithm; biomass fuel

1. Introduction

The severe environmental situation has forced countries to lay out new energy strategies to achieve carbon neutrality. There are still many factors that drive us to seek carbon reduction solutions through renewable energy [1]. Among the renewable energy sources, the development of biomass fuels has been anticipated [2]. Compared with the first generation of biofuels extracted from food crops such as sugar cane and corn [3], the second generation of biofuels synthesized from waste crops, such as corn cobs and other lignocellulose [4], has the advantage of non-competitiveness amongst people for food and is similar in fuel properties to that of traditional fuels. Moreover, the fuel consumption requirements for such fuels should be reduced in terms of greenhouse gas emissions. In addition, the platform molecules [5] possessed by such biofuels are able to be used for the preparation of fuels or high-value-added chemicals, which are highly regarded for their considerable flexibility and can effectively reduce commercial risks. Agricultural waste, such as corn cobs, is the raw material for biofuel in this study, due to the abundance of corn around the study area.

Currently, research on platform molecular compounds prepared from lignocellulosic feedstocks has focused on process improvement for catalytic synthesis [6]. Mailaram et al. [7] studied furan fuels with other biomass compounds as fuel additives. In the study by Khemthong et al. [8], the conversion process of various lignocelluloses and hemicelluloses as renewable energy sources such as biofuels was demonstrated in detail, with the advantages of furfural as a biomass-derived platform being noted in particular. Recently, Jin et al. [9] developed the detailed kinetic reaction mechanism of furfural as a fuel based on the component concentration variation in a jet-stirred reactor (JSR) and laminar combustion rate. In the course of their study, they suggested the possibility of the combustion behavior of furan-based biofuels derived from furfural as a feedstock. Based on the biofuel prepared during the group's pre-process research, an appropriate reaction mechanism will be constructed in this paper for subsequent research.



Citation: Fan, W.; Du, A.; Liu, G.; Liu, Q.; Gao, Y. Study on the Skeleton Mechanism of Second-Generation Biofuels Derived from Platform Molecules. *Processes* **2023**, *11*, 1589. <https://doi.org/10.3390/pr11061589>

Academic Editor: Jiangping Tian

Received: 31 March 2023

Revised: 27 April 2023

Accepted: 2 May 2023

Published: 23 May 2023



Copyright: © 2023 by the authors. Licensee MDPI, Basel, Switzerland. This article is an open access article distributed under the terms and conditions of the Creative Commons Attribution (CC BY) license (<https://creativecommons.org/licenses/by/4.0/>).

There are many corresponding bio-derived fuels [10], and the current common ones include 5-hydroxymethylfurfural (HMF) [11], 2-Methylfuran (MF) [12], and 2,5-dimethylfuran (DMF) [13,14]. The collaborators for this study are the ones who prepare furfuryl alcohol mainly from furfural [15], and furfuryl alcohol is further synthesized into the high-value-added products MF and DMF using copper–silicon-based catalysts [16]. As shown in Figure 1, the synthesis process is a pre-process study between the group and the partner, which is not reflected in this paper. However, the application of such a method of fuel preparation falls under the category of carbon sink [17]. Therefore, this study intends to construct a skeletal chemical reaction mechanism for binary alternative fuels derived from the platform molecule furfural, which consists of MF and DMF, in order to study their combustion characteristics. Thus, the whole research project was completed in a closed loop.

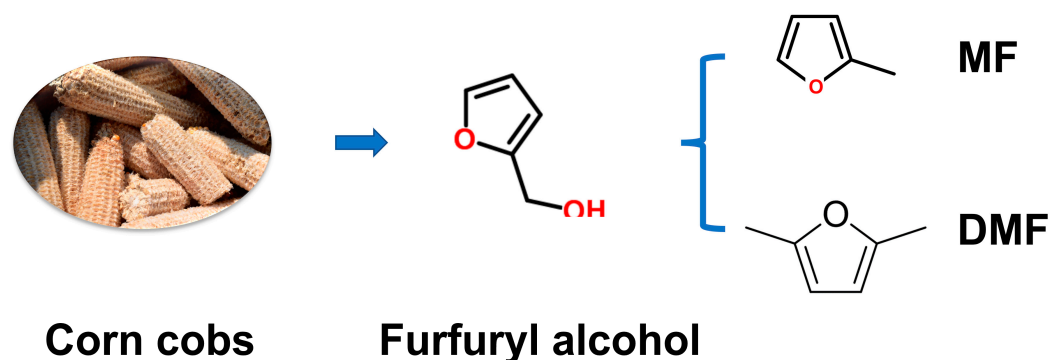


Figure 1. The thematic research for commercial applications.

2. Initial Mechanism

Coupling the C_0 - C_3 sub-mechanism [18] with the fuel sub-mechanism using the decoupling methodology [19], this study proposes the construction of a skeleton mechanism that can respond to the combustion characteristics of DMF and MF based on the DMF sub-mechanism constructed by Somers et al. [20] and the MF sub-mechanism constructed by Tran et al. [21].

2.1. Reaction Path Analysis

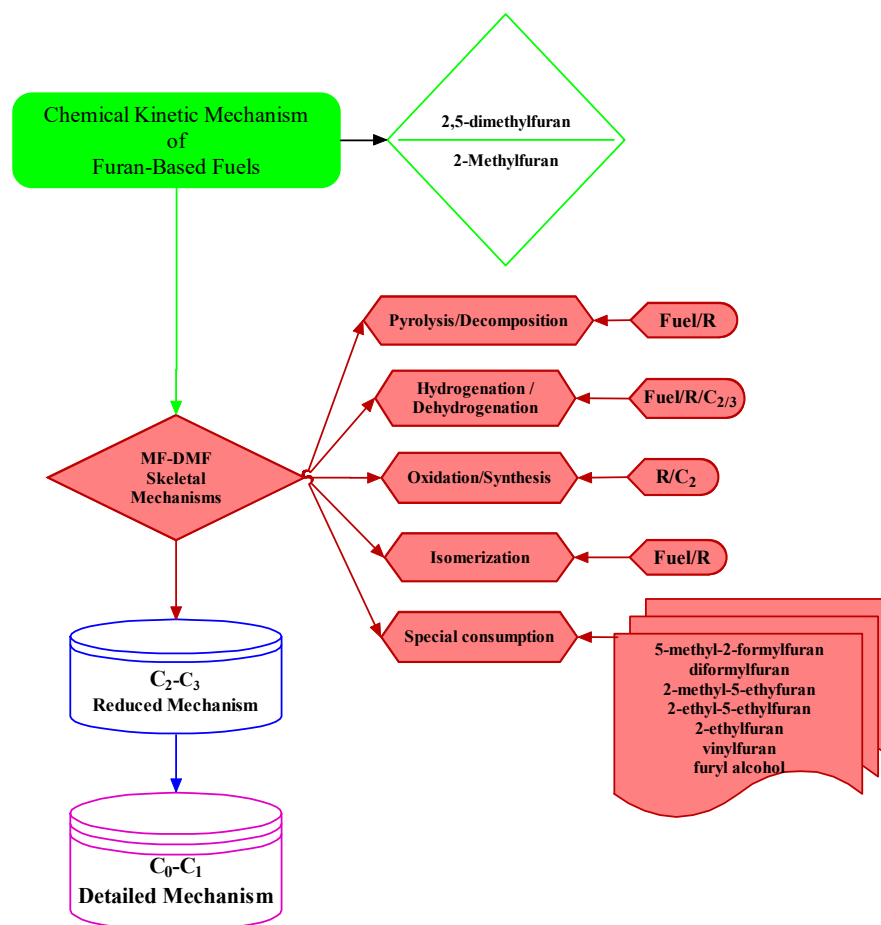
Based on the pathway and reaction coupling sensitivity analysis, it was determined that the initial skeleton mechanism contains 5 major categories and 22 sub-categories of core reactions. The MF-DMF skeleton sub-mechanism reaction types are categorized as shown in Table 1.

2.2. Construction of the Initial Mechanism

In this study, the decoupling methodology was used to construct the chemical reaction mechanism of binary alternative fuels composed of MF-DMF. As shown in Table 1, the MF-DMF sub-mechanism mainly contains 22 types of aggregate and special reactions, which are dominated by C_4+ reactions with a few C_2 - C_3 reactions. As shown in Figure 2, the MF-DMF sub-mechanism is coupled with the C_2 - C_3 simplified mechanism and the C_0 - C_1 detailed mechanism to form the initial chemical reaction mechanism of the binary alternative fuel, which is the decoupling methodology.

Table 1. Reaction categorization.

Major Categories	Sub-Categories	Reaction Number
Pyrolysis/decomposition	Fuel decomposition	r01
	R decomposition	r02
	Intermediate pyrolysis	r03
Hydrogenation/dehydrogenation	C ₂ hydrogenation	r04
	C ₃ hydrogenation	r05
	Fuel dehydrogenation	r06
	R dehydrogenation	r07
	C ₃ dehydrogenation	r08
Oxidation/synthesis	R + O ₂ = ROO	r09
	R + O = RO	r10
	R + HO ₂ = RO + OH	r11
	C ₂ synthesized with OH	r12
	C ₂ synthesized with CH ₃	r13
Isomerization	R-isomerization	r14
Special consumption	5-Methyl-2-formylfuran consumption	r15
	Diformylfuran consumption	r16
	2-Methyl-5-ethylfuran consumption	r17
	2-Ethyl-5-ethylfuran consumption	r18
	2-Ethylfuran consumption	r19
	Vinyl-furan consumption	r20
	Furfuryl alcohol consumption	r21
	Dicarbonyl compounds consumption	r22

**Figure 2.** Framework of the skeleton mechanism. The red section is the main part of this paper.

In this study, the initial mechanism mentioned above was combined and simplified via global sensitivity analysis for some of the reactions using the set sum method. As shown in Table 1, the five major categories in the initial mechanism were combined and simplified into a lumping solution via global sensitivity analysis. These mainly included the lumping of pyrolysis/cracking reactions into r02 reactions, the hydrogenation/dehydrogenation reactions being represented by r04 and R06 reactions, the oxidation/synthesis reactions being mainly expressed by r11 and r12, eliminating the isomerization reactions, with only two types of intermediate product reactions, r15 and r17, being retained to replace all the special consumption reactions of the mechanism. In this way, the reactions of the MF-DMF sub-mechanism in the initial mechanism of the binary alternative fuel were further reduced to seven lumped types.

The reaction pathway of MF-DMF sub-mechanism is summarized in Figure 3. In order to characterize the combustion accurately, the MF part is coupled to the C₃-C₀ sub-mechanism through the following paths: dehydrogenation, oxygenation, re-dehydrogenation, decomposition of CO, and cleavage to small molecules. The pathway is dominated by R1-R13 and R25 reactions. It can also synthesize P14O₃J directly with OH, which later cleaves to methyl vinyl ketone (MVK), which further reacts with hydrogen groups to form C₃-C₀ molecules. The pathway is dominated by R14-R15 reactions. The reaction pathway of DMF is a bit more complex in the mechanism. Firstly, MF can be synthesized by hydrogenation onto DMF, which is the response R24, and then the MF pathway can be used for carbon reduction. Secondly, DMF can also react with OH directly to form MVK, and then the MVK pathway can be used. This path consists of R43 and R16. This pathway is a lumping reaction within the mechanism of this study, which represents multiple reactions such as OH-group, isomerization, and decomposition reactions. Finally, the important intermediate DMF252J is generated from DMF by dehydrogenation. This contains multiple reactions, as follows R17, R16-R31. The intermediate is divided into three pathways through DMF252OJ, CHE21O₄J, and M2E5F, via MF25CHO, P14DE1J, and C5H₆, until coupling with the C₃-C₀ sub-mechanism of the decoupling methodology occurs. The main reactions of these paths are shown in Figure 3. In this way, the initial chemical reaction mechanism of the binary alternative fuel was constructed. The reactions shown in Figure 3 are listed below. The corresponding reactions are listed in Table 2.

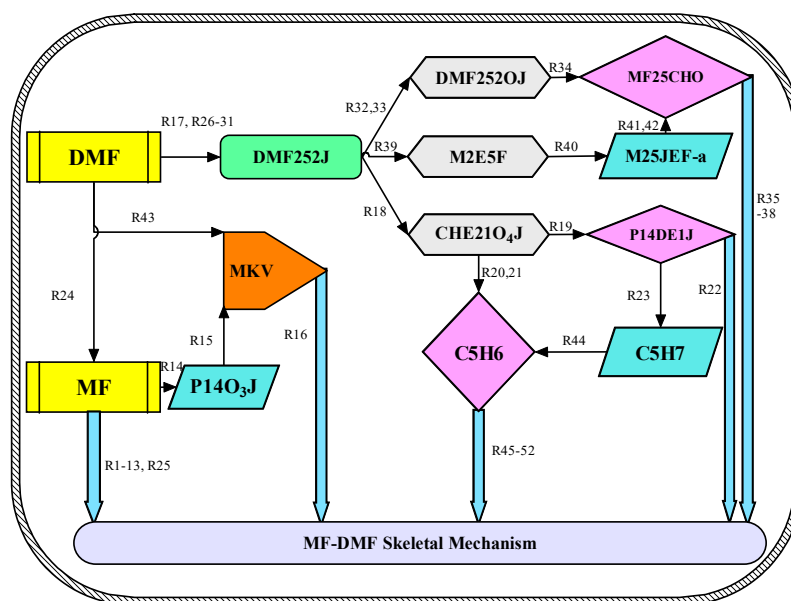


Figure 3. Reaction pathway of MF-DMF skeleton mechanism in binary alternative fuel.

Table 2. The reactions of MF-DMF sub mechanism.

$mf + h = furylch2 + h2$	1.07e + 04	2.730	3.55e + 03	(R01)
$mf + oh = furylch2 + h2o$	3.26e + 04	3.133	2.16e + 03	(R02)
$mf + ch3 = furylch2 + ch4$	1.22e−03	4.290	4.48e + 03	(R03)
$mf + o2 = furylch2 + ho2$	1.60e + 03	3.340	3.47e + 04	(R04)
$mf + o=furylch2 + oh$	1.75e + 10	0.700	5.90e + 03	(R05)
$mf + ho2 = furylch2 + h2o2$	5.10e + 00	3.780	1.23e + 04	(R06)
$ho2 + furylch2 = furylch2o + oh$	3.40e + 35	−6.150	1.60e + 04	(R07)
$ho2 + furylch2 = furylch2o + oh$	1.97e + 40	−8.540	4.80e + 03	(R08)
$furylch2o = furylcho + h$	9.74e + 09	1.440	1.73e + 04	(R09)
$furylcho + oh = furylco + h2o$	7.79e + 13	0.000	0.00e + 00	(R10)
$furylcho + ho2 = furylco + h2o2$	3.00e + 13	0.000	1.10e + 04	(R11)
$furylco = furyl-2 + co$	1.59e + 15	0.000	2.95e + 04	(R12)
$furyl-2 + o2 = ch2chco + co2$	4.33e + 17	−1.390	1.00e + 03	(R13)
$mf + oh = p14o3j$	1.11e + 05	2.450	−7.25e + 03	(R14)
$p14o3j = hco + mvk$	1.07e + 02	2.800	4.43e + 03	(R15)
$mvk + h = c2h4 + ch3co$	4.62e + 11	0.510	2.62e + 03	(R16)
$dmf25(+m) <=> dmf252j + h(+m)$	4.75e + 15	0.070	8.57e + 04	(R17)
$dmf252j = che21o4j$	7.70e + 13	0.157	4.02e + 04	(R18)
$che21o4j = p14de1j + co$	8.17e + 08	1.360	4.38e + 04	(R19)
$che21o4j = chde241o + h$	2.82e + 11	1.020	4.88e + 04	(R20)
$chde241o <=> c5h6 + co$	1.60e + 41	−7.815	5.77e + 04	(R21)
$p14de1j = c2h2 + c3h5$	3.19e + 10	0.000	6.96e + 03	(R22)
$p14de1j = c5h7$	3.56e + 10	0.880	1.61e + 04	(R23)
$dmf25 + h=mf2 + ch3$	5.26e143	−39.13	6.25e + 04	(R24)
$mf2 + oh = ch3co + c2h3cho$	1.11e + 04	2.450	−7.25e + 03	(R25)
$dmf25 + h = dmf252j + h2$	2.95e + 06	2.360	4.48e + 03	(R26)
$dmf25 + oh = dmf252j + h2o$	1.02e + 04	3.130	2.16e + 03	(R27)
$dmf25 + ch3 = dmf252j + ch4$	1.26e + 03	3.020	7.42e + 03	(R28)
$dmf25 + o2 = dmf252j + ho2$	6.25e + 13	0.000	3.53e + 04	(R29)
$dmf25 + o = dmf252j + oh$	1.26e + 12	0.000	3.00e + 03	(R30)
$dmf25 + ho2 = dmf252j + h2o2$	1.98e + 00	3.780	1.23e + 04	(R31)
$dmf252j + ho2 = dmf252oj + oh$	5.00e + 12	0.000	0.00e + 00	(R32)
$dmf252j + ch3o2 = dmf252oj + ch3o$	2.00e + 13	0.000	0.00e + 00	(R33)
$dmf252oj <=> mf25cho + h$	1.13e + 12	0.220	3.38e + 03	(R34)
$mf25cho + ch3 = mf25cjo + ch4$	5.79e−15	8.560	−2.47e + 02	(R35)
$mf25cho + ho2 = mf25cjo + h2o2$	7.05e + 00	3.810	9.25e + 03	(R36)
$mf25cjo = mf25j + co$	4.00e + 14	0.000	2.95e + 04	(R37)
$mf25j = c3h4 + hcco$	1.02e + 14	0.000	2.69e + 04	(R38)
$dmf252j + ch3 = m2e5f$	1.25e + 13	0.000	0.00e + 00	(R39)
$m2e5f + ch3 = m25jef-a + ch4$	2.26e + 03	2.890	5.77e + 03	(R40)
$m25jef-a + ho2 => mf25cho + oh + ch3$	5.00e + 12	0.000	0.00e + 00	(R41)
$m25jef-a + ch3o2 => mf25cho + ch3o + ch3$	5.00e + 12	0.000	0.00e + 00	(R42)

Table 2. Cont.

$\text{dmf25} + \text{oh} = \text{mvk} + \text{ch3co}$	$2.21\text{e} + 04$	2.450	$-7.25\text{e} + 03$	(R43)
$\text{c5h7} + \text{o2} = \text{c5h6} + \text{ho2}$	$1.30\text{e} + 15$	-1.070	$9.53\text{e} + 03$	(R44)
$\text{c5h6} + \text{o} = \text{c5h5} + \text{oh}$	$4.77\text{e} + 04$	2.700	$1.11\text{e} + 03$	(R45)
$\text{c5h6} + \text{oh} = \text{c5h5} + \text{h2o}$	$3.08\text{e} + 06$	2.000	$0.00\text{e} + 00$	(R46)
$\text{c5h6} + \text{o} \Rightarrow \text{c2h4} + \text{c2h2} + \text{co}$	$3.89\text{e} + 08$	1.360	$8.87\text{e} + 02$	(R47)
$\text{c5h5} + \text{oh} \Leftrightarrow \text{c5h4oh} + \text{h}$	$3.50\text{e} + 57$	-12.18	$4.84\text{e} + 04$	(R48)
$\text{c5h5} + \text{o} \Rightarrow \text{c2h2} + \text{c2h3} + \text{co}$	$9.20\text{e} + 13$	-0.170	$4.40\text{e} + 02$	(R49)
$\text{c5h4oh} \Leftrightarrow \text{c5h4o} + \text{h}$	$2.10\text{e} + 13$	0.000	$5.40\text{e} + 04$	(R50)
$\text{c5h4o} \Rightarrow \text{c2h2} + \text{c2h2} + \text{co}$	$5.70\text{e} + 32$	-6.760	$6.85\text{e} + 04$	(R51)
$\text{c5h4o} \Rightarrow \text{c2h2} + \text{c2h2} + \text{co}$	$6.20\text{e} + 41$	-7.870	$9.87\text{e} + 04$	(R52)

Note: The above format is the Chemkin adaptation. Specific content can be found in the Supplementary Materials.

3. Optimization Mechanism with Genetic Algorithm

In this subsection, the initial mechanism of the binary alternative fuel is optimized by the non-inferiority solution ranking genetic algorithm program (NSGA-II), which is commonly used by the group [22]. The core of optimization lies in the rational adjustment of the reaction rate coefficient of the MF-DMF sub-mechanism.

3.1. Genetic Algorithm

The optimization principle is to set the rate coefficient of the lumping reaction to be adjusted as a priority. By comparing the experimental results of similar fuels in the shock tube (ST) and JSR, which allows the mechanism to simulate ignition and combustion characteristics of a fuel accurately [23]. As shown in Figure 4, the initial mechanism is optimized iteratively via the following steps:

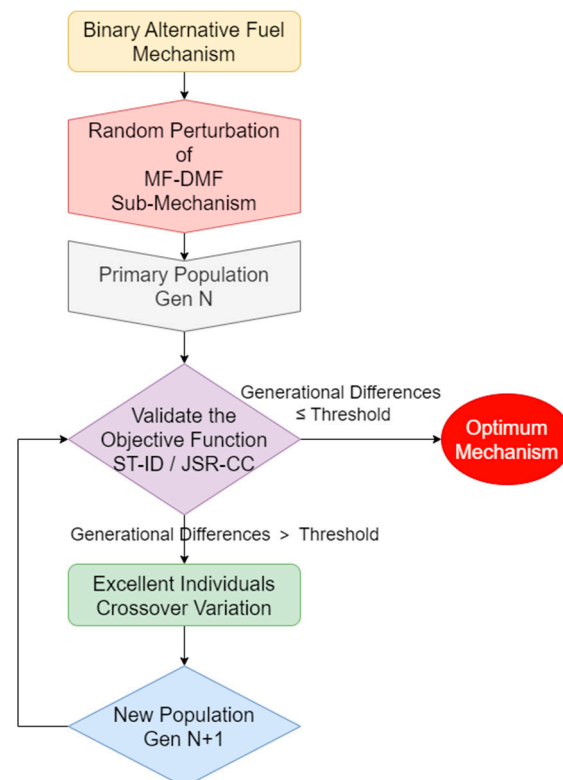


Figure 4. Flowchart of NSGA-II [22].

- (1) Adjusting the parameters of the Arrhenius equation for the MF-DMF sub-mechanism in the initial mechanism within a certain range, multiple mechanisms are randomly generated to constitute the primitive population Gen N .
- (2) By invoking the Chemkin-Pro program, the genetic algorithm analyzes the prediction accuracy of ignition delay (ID) and component concentration (CC) for each mechanism in the current population and also determines whether to continue the iteration or to output the results based on the difference between the prediction accuracy of the upper and lower generations of the population.
- (3) If the predicted difference between generations is greater than a threshold, the dominant individuals in the population of the current generation are selected for inheritance. These individuals are subjected to non-dominant stratification and crowding measures via selection, crossover, and mutation operations, and are ranked in order of superiority. The multiple new mechanisms thus generated serve as the offspring population, Gen $N + 1$.
- (4) Then, the calculation of steps (2) and (3) is repeated for Gen $N + 1$ until the reproduction of intergenerational difference is not greater than a threshold. Genetic termination then occurs and the final result is output as the optimal mechanism.

3.2. Optimal Mechanism

The optimization process of this algorithm is expressed in Equations (1)–(3) for the fitting functions of the ID in ST and the CC in JSR, respectively. Additionally, the optimized iterative evolution process is represented by a Pareto front [24] diagram as shown in Figure 5.

$$f_{ID} = \sum_{i=1}^{N_1} \left| \frac{\tau'_i - \tau_i^0}{\tau_i^0} \right| \quad (1)$$

$$f_{CC} = \sum_{j=1}^{N_2} \sum_{k=1}^{N_3} \left| \frac{C'_{j,k} - C_{j,k}^0}{C_{j,k}^{avg}} \right| \quad (2)$$

$$C_{avg} = \frac{C_y + C_{max}}{2} \quad (3)$$

where f_{ID} and f_{CC} represent the prediction accuracy fitting functions of the skeleton mechanism to ID and CC, respectively; τ represents the ignition delay; C represents the concentration of the substance component; the upper corner markers 0 and ' represent the experimental and predicted values, respectively; the lower corner marker i represents the i th ignition delay; the subscript j represents the j th component; the subscript k represents the k th temperature measurement point for that component; N represents the total amount of data, and the subscripts 1, 2 and 3 are used to indicate the ID, CC and measurement points in JSR, respectively. $C_{j,k}^{avg}$ in Equation (2) is obtained from Equation (3), where the subscript y represents the experimental concentration of the y th component at a certain temperature and the subscript max represents the maximum experimental concentration of the component at the same temperature.

If the above optimization process also has multiple sets of parallel experimental results, an additional set of merging operations for parallel experimental results is required.

Figure 5 shows the comparative results of the Pareto fronts for the 100th, 200th, 500th, 750th and 1000th generations in the genetic algorithm optimization. As seen in Figure 5, the mechanism converged to the optimal Pareto front at the 750th generation as the number of generations increased. Instead, further iterations tended to lead to biased iteration results, as shown in the 1000th generation. This has been mentioned in many studies [25,26], and this study suggests that it is possible that a flawed elite selection procedure led to sampling errors that affected the iterative robustness [27]. For this study only, the optimization results of the 750th generation can be used for subsequent simulations, which possess more desirable convergence.

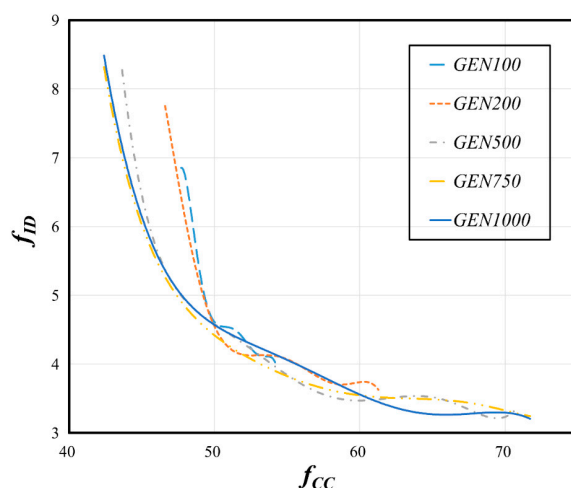


Figure 5. The comparison of Pareto fronts between generations.

4. Validation of the Mechanism

This study focuses on the development of second-generation biomass fuels based on furfural-derived MF and DMF. Since there is a lack of experimental data on the combustion of MF-DMF directly, the following validation will be carried out separately for similar experimental parameters of each substance under a wide range of conditions. The validation process includes several validation parameters for both substances that reflect the performance of the mechanism.

4.1. Ignition Delay

The ignition delay is one of the important parameters that describe the combustion characteristics of a fuel. Its common experimental devices are ST and a rapid compression machine (RCM) to maintain a stable response test under the operating conditions approximating the engine. This section will verify the prediction accuracy of the mechanism for such experimental results.

4.1.1. ID in ST

Due to the lack of experimental results for this alternative fuel, the present verification compares the experimental results of ignition delay, which was measured in a ST by Uygun et al. for MF [12] and Somers et al. for DMF [20]. As shown in Figure 6, the optimized mechanism of the binary alternative fuel has a good prediction accuracy for the ID of MF and DMF in ST at stoichiometric, temperature intervals of 800–1250 K, with pressure taken as 20, 40, and 80 bar. The experimental uncertainties are all 20%. The advantages of this mechanism for the ID prediction of DMF are obvious. Additionally, for MF, the ID prediction is better in the low-temperature region. However, there are some deviations in the prediction of the ID for MF under high temperatures and for DMF in the low-pressure and low-temperature regions.

In this study, the mechanism was also analyzed with predictive accuracy specifically for two core fuels under low-pressure and high-temperature conditions. On the one hand, the prediction accuracy of this mechanism for MF at a low pressure and high temperature is tested; on the other hand, the prediction ability of DMF at an extremely low pressure and high temperature is further analyzed. The verification results are shown in Figure 7.

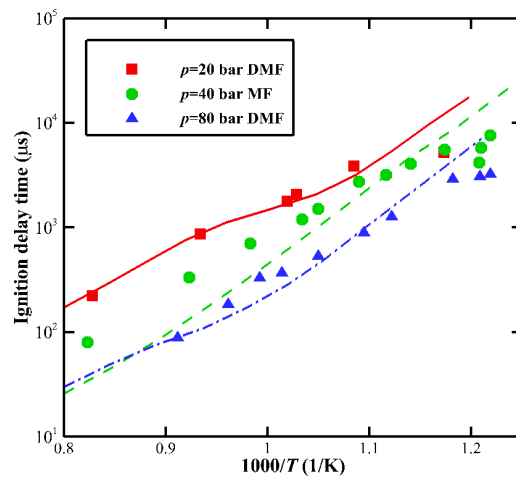


Figure 6. Experimental and predicted results of ID obtained for alternative fuel/air mixtures in a ST at $p = 20, 40,$ and 80 bar and stoichiometric results. The dots are the experimental results [12,20] and the lines are the predicted results.

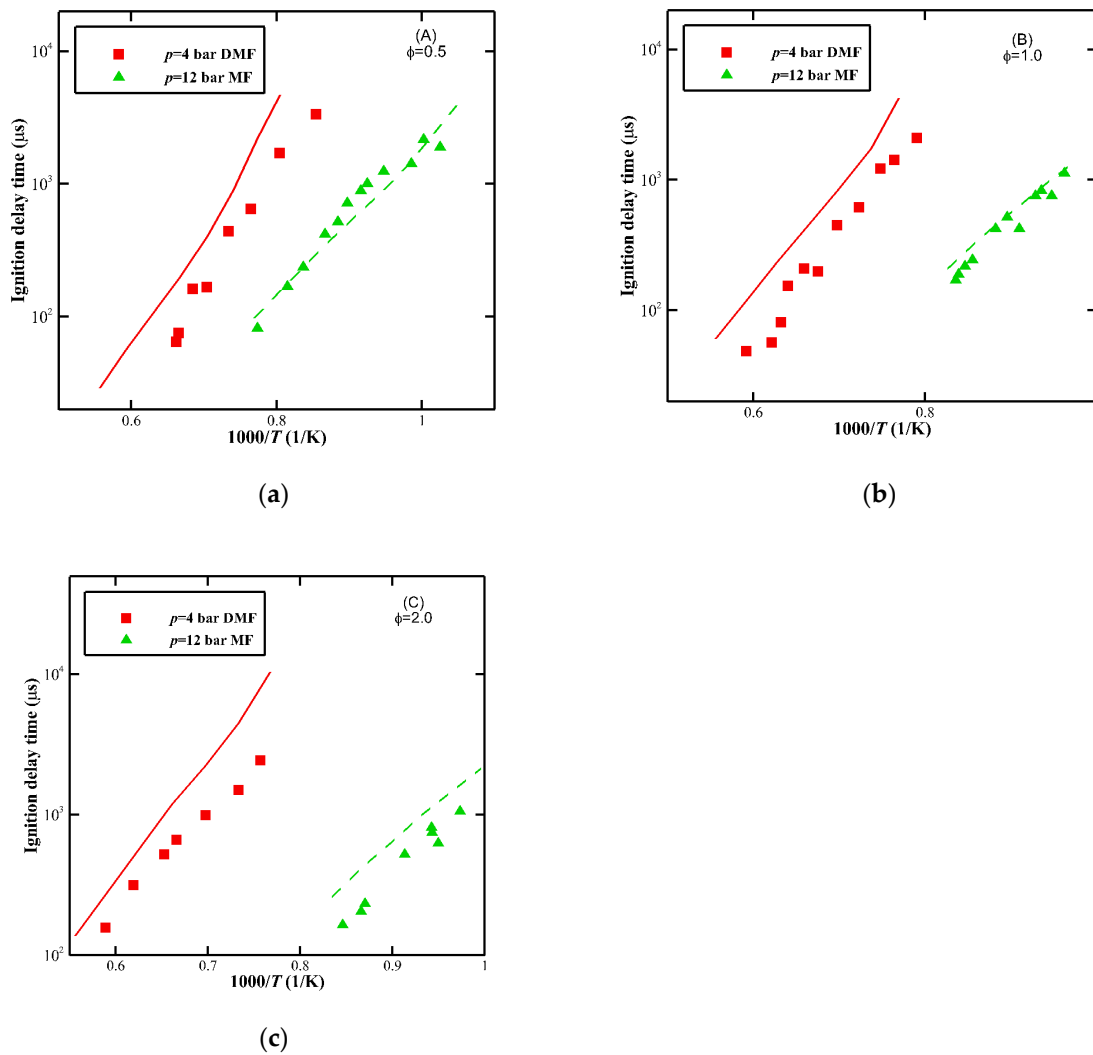


Figure 7. Experimental and predicted results of ID obtained for alternative fuel/oxygen mixtures in a ST at $\phi = 0.5\text{--}2.0$ and $p = 4$ and 12 bar, respectively. (a): $\phi = 0.5$; (b): $\phi = 1.0$; (c): $\phi = 2.0$. The dots are the experimental results [28,29] and the lines are the predicted results.

As shown in Figure 7, the optimized skeleton mechanism of the binary alternative fuel was tested under low pressure for the ID of MF and DMF, respectively. The uncertainty of these two sets of experimental data is about 21% and 30%, respectively. As mentioned by Somers et al. [20], the uncertainty is a systematic problem that encompasses fluctuations in pressure, temperature, measurement methods and other factors. This mechanism describes the ID of MF mixed with oxygen under a low equivalent ratio better, but there is some bias in the prediction for the opposite conditions. Meanwhile, the prediction accuracy of the mechanism for DMF under low-pressure and high-temperature conditions has significant deviations. Among them, the prediction accuracy is better around 1400 °C at low equivalent ratios and shifts toward the high-temperature region at high equivalent ratios. As mentioned by Li et al. [30], the above discrepancies are mainly caused by the differences between the substances and reaction paths in the skeleton mechanism and the actual fuel.

4.1.2. ID in RCM

Usually, the ST mainly studies the ignition characteristics of the fuel at high temperatures [31], while the characteristics of the low-temperature region are often analyzed via RCM [32]. Since RCM belongs to piston isentropic compression heating, it is more informative in some operating conditions compared to ST with adiabatic non-isentropic heating.

The ID prediction accuracy of DMF/O₂ mixtures in RCM using this mechanism is shown in Figure 8. Considering the experimental uncertainty of 11%, it can be seen that the mechanism is more accurate at predicting the ignition delay between 830–1100 K, which is consistent with the piston compression. However, the mechanism shows significant prediction deviation at low equivalent ratios and temperatures of less than 830 K. Since the optimization process of the mechanism mainly refers to high temperature, high pressure and stoichiometric ratios, resulting in some low temperature, low pressure or low equivalence ratio reaction effects are not accurately considered, thus affecting the prediction accuracy under such conditions. This may be related to the restricted engine ignition temperature and the characteristics of the binary alternative fuel.

4.2. Verification of Component Concentrations

Another major reference for the optimization mechanism in this study is the prediction accuracy of the component concentration during fuel combustion. Combined with the prediction accuracy of this parameter, it can fully reflect the performance of the optimization mechanism.

4.2.1. Jet-Stirred Reactor

The mechanism was validated by predicting the component concentrations in the JSR, and the experimental results used for the validation were the data measured by Somers et al. [20] on the variation of the main component concentrations in the JSR for DMF/air mixtures. There is an uncertainty of about 15% in these data. Due to a large number of combustion components, this section only selects the concentrations of some key components for comparative analysis.

Figure 9 shows the results of the analysis of several major component concentrations of DMF/air mixtures predicted by the optimization mechanism in JSR compared with experimental data, including two reactants, two products, and two major intermediates, with working conditions of $\varphi = 0.5\text{--}2.0$, $p = 10$ bar and $T = 700\text{--}1250$ K. As can be seen from Figure 9, the mechanism predicts component concentrations lower than the experimental values at low equivalence ratios and partially higher concentrations at high equivalence ratios, while the prediction accuracy is excellent upon the performance of stoichiometry. When predicting oxygen consumption, this mechanism predicts better under medium to high equivalence ratios, while the prediction is high under low equivalence ratios. This mechanism is able to predict both H₂O and CO₂ well at low to medium temperatures, with minor deviations at high temperatures. As far as the prediction results of two intermediates, CO and CH₂O, selected in this study, the mechanism is able to predict accurately except for

a slightly higher prediction of CH_2O at low equivalence ratios and low temperatures. Considering the small order of magnitude of the component concentrations and the uncertainty of the experimental data [20], this mechanism is basically able to predict the component concentrations reliably.

4.2.2. Premixed Laminar Flame

In addition to analyzing the component concentration trends during fuel oxidation at low temperatures in the JSR, this subsection will also compare the evolutionary predictions for the component concentration after fuel combustion and expect better predictions.

Figure 10 shows the results of the analysis of several major component concentrations of DMF/oxygen mixtures predicted by the optimization mechanism in a premixed laminar burner compared with the experimental data, including two reactants, two products, and one major intermediate, with working conditions of $\phi = 1.0$ and 1.7, $p = 20$ and 40 mbar, and a distance from the burner from 0 to 25 mm. As can be seen in Figure 10, the mechanism is slightly faulty when predicting the trend of substance concentration in premixed laminar flames at chemical equivalent ratios and low pressures, while it performs quite well in predicting the trend of substance concentration in premixed laminar flames at high equivalent ratios and higher pressures. It is shown that the mechanism can better predict the changes in component concentrations during fuel combustion in engines.

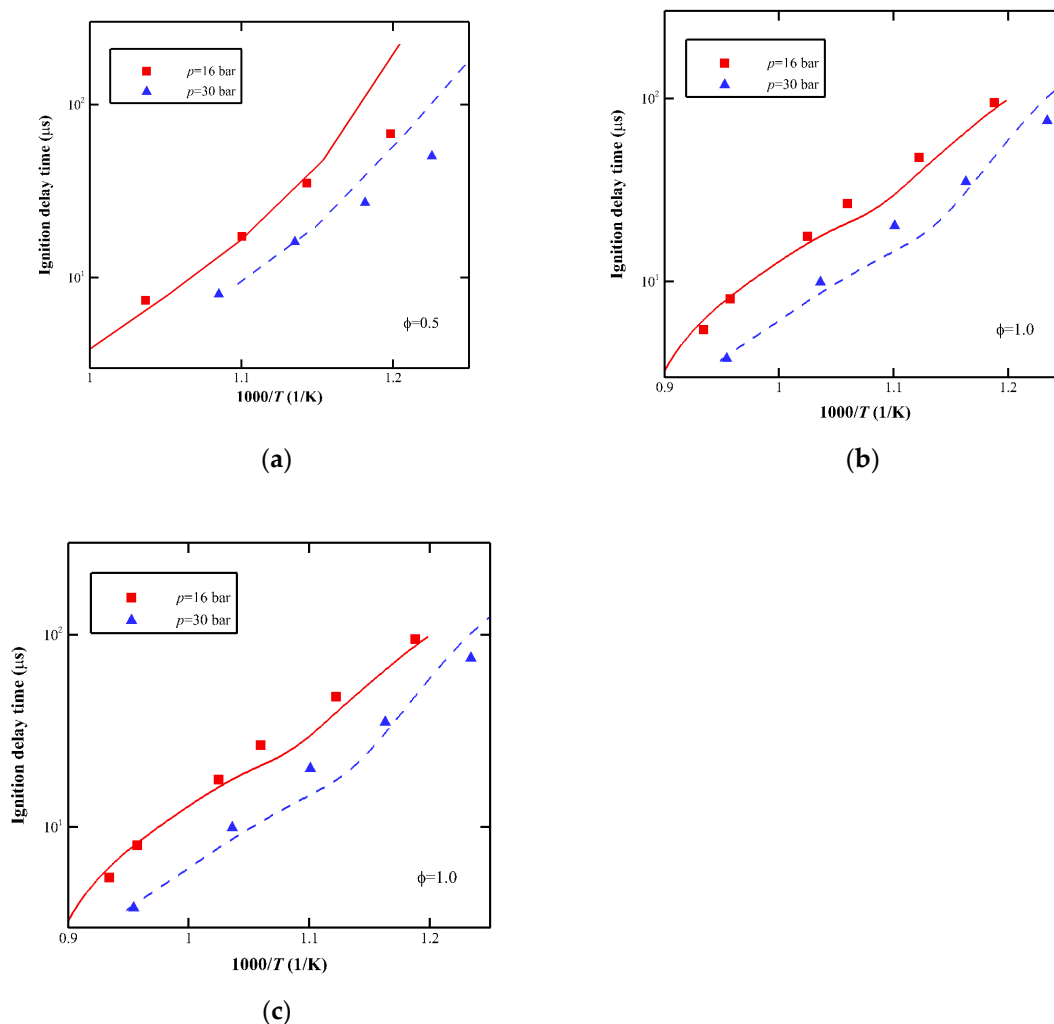


Figure 8. Experimental and predicted results of ID obtained for alternative fuel/oxygen mixtures in a RCM at $\phi = 0.5$ – 2.0 and $p = 16$ and 30 bar, respectively. (a): $\phi = 0.5$; (b): $\phi = 1.0$; (c): $\phi = 2.0$. The dots are the experimental results [33] and the lines are the predicted results.

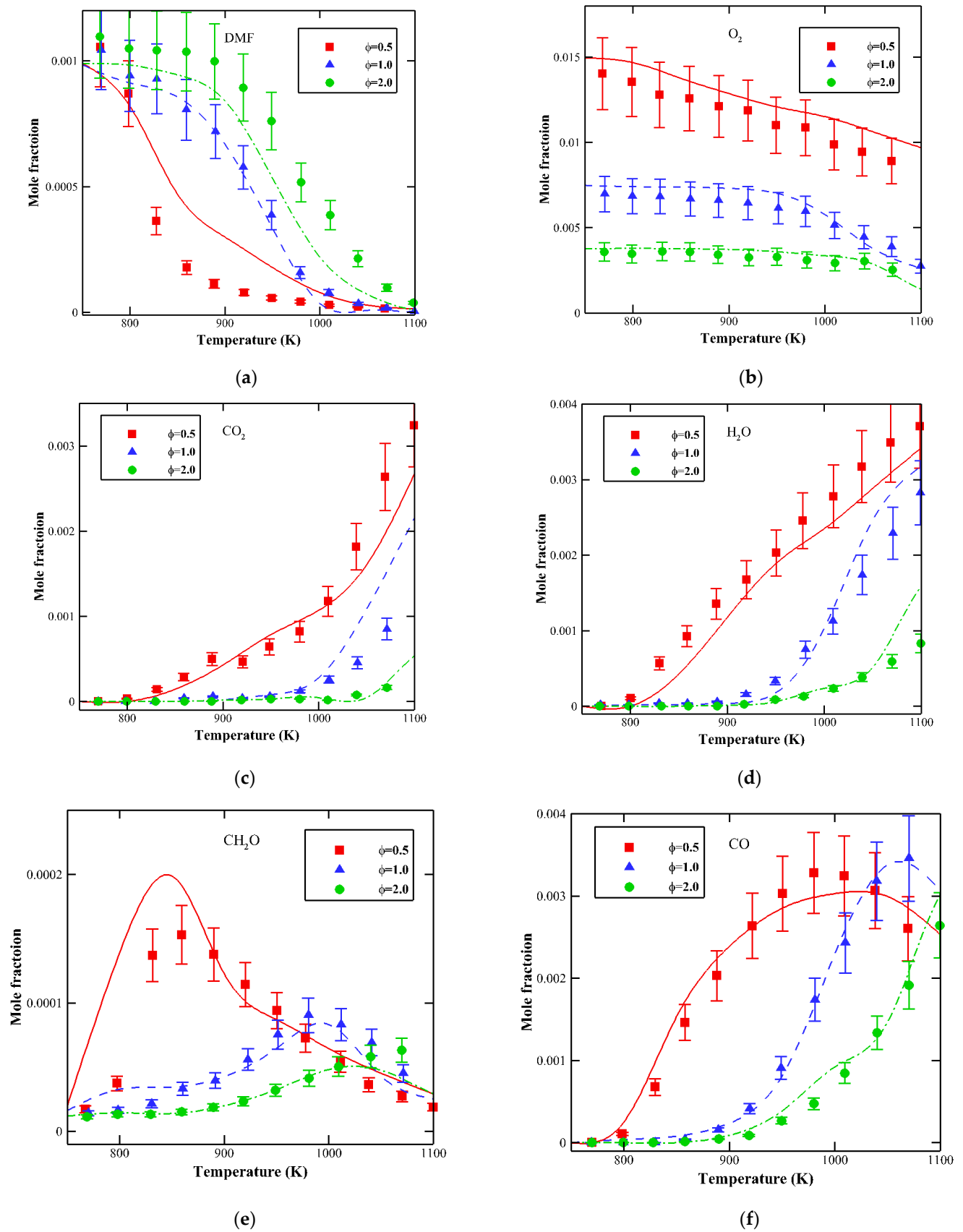


Figure 9. Experimental and predicted results of CC obtained for alternative fuel/air mixtures in a JSR at $\phi = 0.5$ – 2.0 and $p = 10$ bar. (a): DMF; (b): O_2 ; (c): CO_2 ; (d): H_2O ; (e): CH_2O ; (f): CO. The dots are the experimental results [20] and the lines are the predicted results.

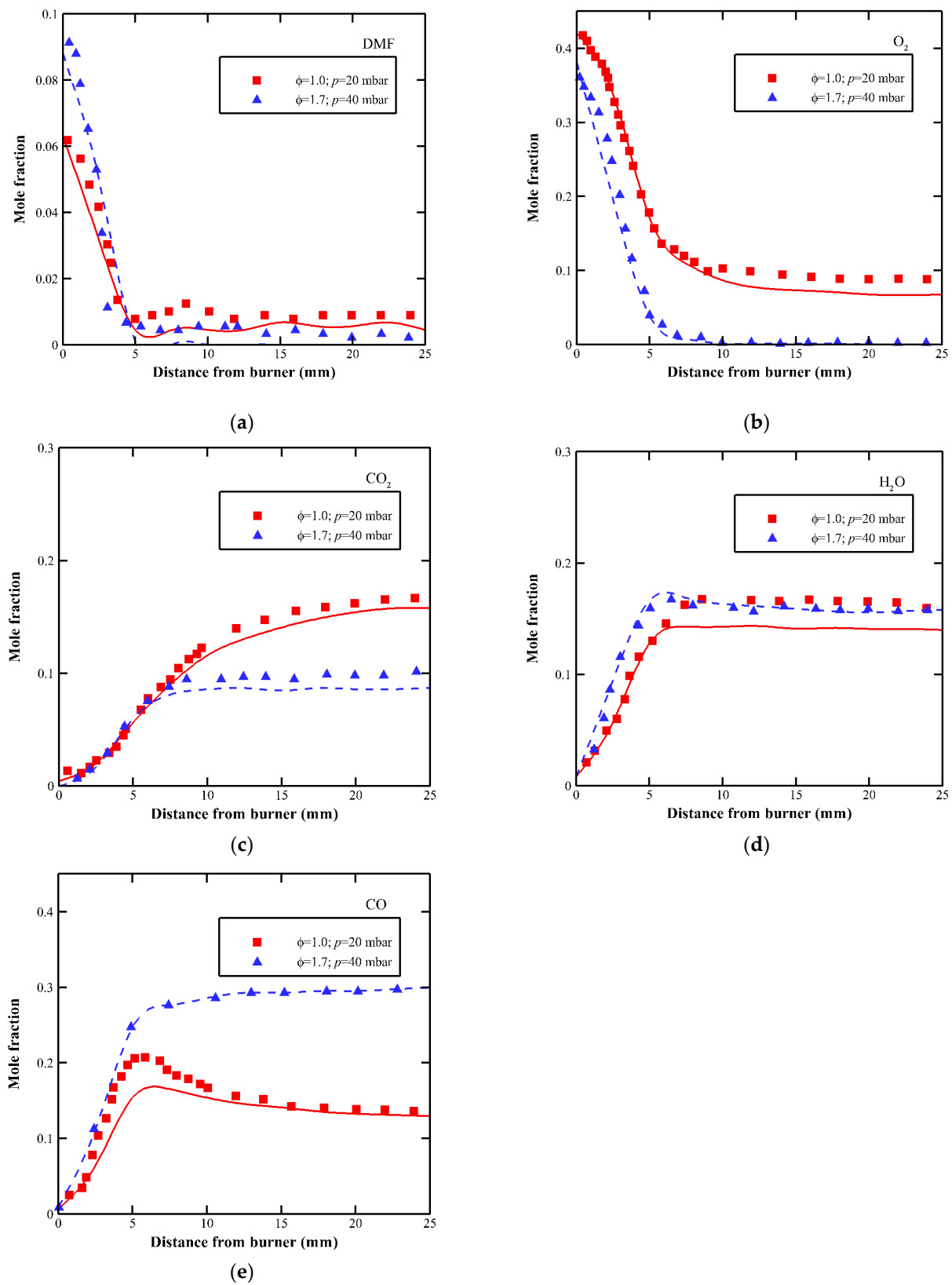


Figure 10. Experimental and predicted results of CC obtained for alternative fuel/oxygen mixtures in a premixed laminar burner at $\phi = 1.0$ and 1.7 , $p = 20$ and 40 mbar. (a): DMF; (b): O_2 ; (c): CO_2 ; (d): H_2O ; (e): CO. The dots are the experimental results [34] and the lines are the predicted results.

4.3. Laminar Flame Speed

At the end of this study, this mechanism was also used to calculate the premixed laminar flame speed of the DMF/oxygen mixture at $p = 1$ atm in an adiabatic burner, and the predicted results are shown in Figure 11. The uncertainty of the experimental results in Figure 11 are measured by the following equation [20]:

$$U = (LFS \times 0.015) + 0.4 \quad (4)$$

where U stands for uncertainty and LFS is the laminar flame speed.

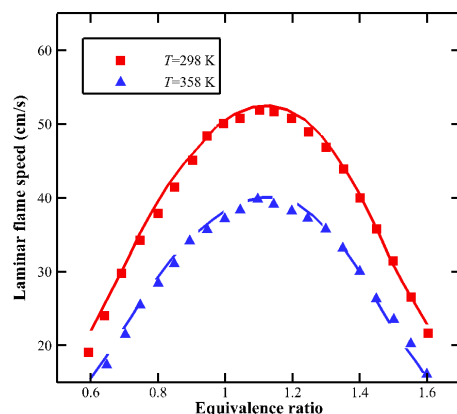


Figure 11. Calculated results of alternative fuel/oxygen mixtures on laminar flame speed. The dots are the experimental results [20] and the lines are the calculated results.

As shown in Figure 11, this mechanism has excellent accuracy in predicting the laminar flame speed of DMF/oxygen mixtures at $T = 298$ and 358 K, where the effect of experimental uncertainty is almost negligible. Combining the previous analysis with this, it is confirmed that the mechanism has the ability to predict the combustion characteristics of the binary alternative fuel.

As shown in Figure 12, the present study constructs mechanisms that describe well the experimental results of Ma et al. [35] but deviate considerably from the results of Wu et al. [36] for the same conditions due to the differences of the experimental technique leading to some differences in experimental data under the same operating conditions. This measurement uncertainty can make it difficult for the mechanism to fit the laminar flame speed for each fuel well [37].

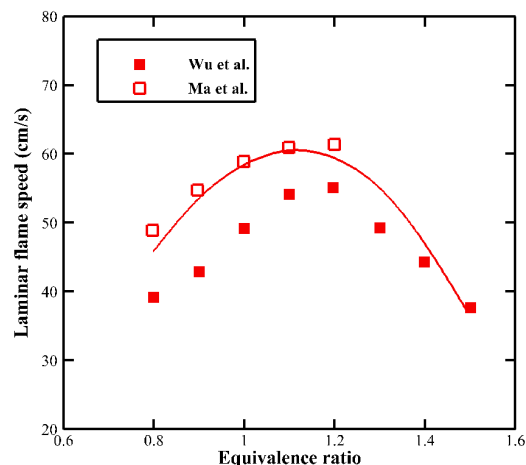


Figure 12. Calculated results of alternative fuel/oxygen mixtures on laminar flame speed at 393 K and 1 bar. The solid dots are the experimental results of Wu et al. [35], the hollow dots are the experimental results of Ma et al. [36] and the lines are the calculated results.

5. Conclusions

The subject of this article is a binary alternative fuel, which consists of furan-based biomass fuels synthesized from lignocellulose, 2-methylfuran and 2,5-dimethylfuran. A skeleton mechanism conforming to its combustion characteristics was constructed using the decoupling methodology, the mechanism was optimized via a genetic algorithm, and an optimal mechanism consisting of 67 components and 228 reactions was obtained. In this study, the final optimized skeleton mechanism of the alternative fuel was used to predict the ignition delay in ST and RCM, the component concentration in JSR and premixed laminar burner, and the laminar flame speed, respectively. Despite the lack of experimental data for 2-methylfuran, via a comparison of the available experimental data, it was found that the mechanism obtained a desirable prediction accuracy at $\varphi = 0.5\text{--}2.0$, $p \geq 20$ bar, and $T = 800\text{--}1200$ K in the several verifications mentioned above. However, some discrepancies still exist. In this study, the simplification and optimization of the mechanism is focused on the engine conditions, which may neglect some relatively important reactions at conventional conditions and lead to errors in the experimental values and simulated values using the skeleton mechanism under non-engine conditions. In the future, more extreme experimental data can be introduced to improve the performance of the current skeleton mechanism. In addition, when applicable 2-methylfuran experimental data are available, the prediction of relevant parameters can be investigated.

Supplementary Materials: The following supporting information can be downloaded at <https://www.mdpi.com/article/10.3390/pr11061589/s1>.

Author Contributions: Conceptualization and methodology, W.F.; software, G.L.; validation, A.D.; formal analysis, Q.L.; data curation, Y.G. All authors have read and agreed to the published version of the manuscript.

Funding: This research was funded by The Science and Technology Department of Henan Province (grant number 212102311151) and The Henan Young Key Teacher Project (grant number 2021GGJS180).

Informed Consent Statement: Informed consent was obtained from all subjects involved in the study.

Data Availability Statement: The data presented in this study are available in the Supplementary Materials.

Conflicts of Interest: The authors declare no conflict of interest.

References

1. Centi, G.; Lanzafame, P.; Perathoner, S. Analysis of the alternative routes in the catalytic transformation of lignocellulosic materials. *Catal. Today* **2011**, *167*, 14–30. [[CrossRef](#)]
2. Kim, S.; Im, H.; Yu, J.; Kim, K.; Kim, M.; Lee, T. Biofuel production from Euglena: Current status and techno-economic perspectives. *Bioresour. Technol.* **2023**, *371*, 128582. [[CrossRef](#)] [[PubMed](#)]
3. Brêda, G.C.; Aguiéiras, E.C.G.; Cipolatti, E.P.; Greco-Duarte, J.; Collaço, A.C.d.A.; Costa Cavalcanti, E.D.; de Castro, A.M.; Freire, D.M.G. Current approaches to use oil crops by-products for biodiesel and biolubricant production: Focus on biocatalysis. *Bioresour. Technol. Rep.* **2022**, *18*, 101030. [[CrossRef](#)]
4. Yong, K.J.; Wu, T.Y. Second-generation bioenergy from oilseed crop residues: Recent technologies, techno-economic assessments and policies. *Energy Convers. Manag.* **2022**, *267*, 115869. [[CrossRef](#)]
5. Melero, J.A.; Morales, G.; Paniagua, M.; López-Aguado, C. Chapter 11—Chemical routes for the conversion of cellulosic platform molecules into high-energy-density biofuels. In *Handbook of Biofuels Production*, 3rd ed.; Luque, R., Lin, C.S.K., Wilson, K., Du, C., Eds.; Woodhead Publishing: Sawston, UK, 2023; pp. 361–397. [[CrossRef](#)]
6. Awasthi, M.K.; Sar, T.; Gowd, S.C.; Rajendran, K.; Kumar, V.; Sarsaiya, S.; Li, Y.; Sindhu, R.; Binod, P.; Zhang, Z.; et al. A comprehensive review on thermochemical, and biochemical conversion methods of lignocellulosic biomass into valuable end product. *Fuel* **2023**, *342*, 127790. [[CrossRef](#)]
7. Mailaram, S.; Kumar, P.; Kunamalla, A.; Saklecha, P.; Maity, S.K. 3—Biomass, biorefinery, and biofuels. In *Sustainable Fuel Technologies Handbook*; Dutta, S., Mustansar Hussain, C., Eds.; Academic Press: Cambridge, MA, USA, 2021; pp. 51–87. [[CrossRef](#)]
8. Khemthong, P.; Yimsukanan, C.; Narkkun, T.; Srifa, A.; Witoon, T.; Pongchaiphon, S.; Kiatphuengporn, S.; Faungnawakij, K. Advances in catalytic production of value-added biochemicals and biofuels via furfural platform derived lignocellulosic biomass. *Biomass Bioenergy* **2021**, *148*, 106033. [[CrossRef](#)]

9. Jin, Z.-H.; Yu, D.; Liu, Y.-X.; Tian, Z.-Y.; Richter, S.; Braun-Unkhoff, M.; Naumann, C.; Yang, J.-Z. An experimental investigation of furfural oxidation and the development of a comprehensive combustion model. *Combust. Flame* **2021**, *226*, 200–210. [[CrossRef](#)]
10. Kwon, H.; Lapointe, S.; Zhang, K.; Wagnon, S.W.; Pitz, W.J.; Zhu, J.; McEnally, C.S.; Pfefferle, L.D.; Xuan, Y. Sooting tendencies of 20 bio-derived fuels for advanced spark-ignition engines. *Fuel* **2020**, *276*, 118059. [[CrossRef](#)]
11. Nishimura, S.; Ikeda, N.; Ebitani, K. Selective hydrogenation of biomass-derived 5-hydroxymethylfurfural (HMF) to 2,5-dimethylfuran (DMF) under atmospheric hydrogen pressure over carbon supported PdAu bimetallic catalyst. *Catal. Today* **2014**, *232*, 89–98. [[CrossRef](#)]
12. Uygun, Y.; Ishihara, S.; Olivier, H. A high pressure ignition delay time study of 2-methylfuran and tetrahydrofuran in shock tubes. *Combust. Flame* **2014**, *161*, 2519–2530. [[CrossRef](#)]
13. Wu, X.; Huang, Z.; Jin, C.; Wang, X.; Wei, L. Laminar Burning Velocities and Markstein Lengths of 2,5-Dimethylfuran-Air Premixed Flames at Elevated Temperatures. *Combust. Sci. Technol.* **2010**, *183*, 220–237. [[CrossRef](#)]
14. Hoang, A.T.; Nižetić, S.; Ölçer, A.I. 2,5-Dimethylfuran (DMF) as a promising biofuel for the spark ignition engine application: A comparative analysis and review. *Fuel* **2021**, *285*, 119140. [[CrossRef](#)]
15. An, Z.; Li, J. Recent advances in the catalytic transfer hydrogenation of furfural to furfuryl alcohol over heterogeneous catalysts. *Green Chem.* **2022**, *24*, 1780–1808. [[CrossRef](#)]
16. Jiménez-Gómez, C.P.; Cecilia, J.A.; Alba-Rubio, A.C.; Cassidy, A.; Moreno-Tost, R.; García-Sancho, C.; Maireles-Torres, P. Tailoring the selectivity of Cu-based catalysts in the furfural hydrogenation reaction: Influence of the morphology of the silica support. *Fuel* **2022**, *319*, 123827. [[CrossRef](#)]
17. Li, M.; Peng, J.; Lu, Z.; Zhu, P. Research progress on carbon sources and sinks of farmland ecosystems. *Resour. Environ. Sustain.* **2023**, *11*, 100099. [[CrossRef](#)]
18. Fan, W.; Yang, S.; Xu, K.; Zhu, M.; Xu, J. Analysis of the Ignition Behavior Based on Similarity Factor Method. *Energies* **2021**, *14*, 873. [[CrossRef](#)]
19. Fan, W.; Jia, M.; Chang, Y.; Xie, M. Understanding the Relationship between Cetane Number and the Ignition Delay in Shock Tubes for Different Fuels Based on a Skeletal Primary Reference Fuel (n-Hexadecane/Iso-cetane) Mechanism. *Energy Fuels* **2015**, *29*, 150416074949000. [[CrossRef](#)]
20. Somers, K.P.; Simmie, J.M.; Gillespie, F.; Conroy, C.; Black, G.; Metcalfe, W.K.; Battin-Leclerc, F.; Dirrenberger, P.; Herbinet, O.; Glaude, P.-A.; et al. A comprehensive experimental and detailed chemical kinetic modelling study of 2,5-dimethylfuran pyrolysis and oxidation. *Combust. Flame* **2013**, *160*, 2291–2318. [[CrossRef](#)]
21. Tran, L.-S.; Wang, Z.; Carstensen, H.-H.; Hemken, C.; Battin-Leclerc, F.; Kohse-Höinghaus, K. Comparative experimental and modeling study of the low- to moderate-temperature oxidation chemistry of 2,5-dimethylfuran, 2-methylfuran, and furan. *Combust. Flame* **2017**, *181*, 251–269. [[CrossRef](#)]
22. Fan, W.; Chang, Y.; Niu, B.; Wang, Y. Numerical Simulation of the Combustion Characteristics of Aviation Kerosene Based on Non-dominated Sorting Genetic Algorithm. *J. Henan Inst. Technol.* **2020**, *28*, 9.
23. Niu, B.; Jia, M.; Xu, G.; Chang, Y.; Xie, M. Efficient Approach for the Optimization of Skeletal Chemical Mechanisms with Multiobjective Genetic Algorithm. *Energy Fuels* **2018**, *32*, 7086–7102. [[CrossRef](#)]
24. Xu, Y.; Zhang, H.; Huang, L.; Qu, R.; Nojima, Y. A Pareto Front grid guided multi-objective evolutionary algorithm. *Appl. Soft Comput.* **2023**, *136*, 110095. [[CrossRef](#)]
25. Pandey, H.M. 3—State of the art: Genetic algorithms and premature convergence. In *State of the Art on Grammatical Inference Using Evolutionary Method*; Pandey, H.M., Ed.; Academic Press: Cambridge, MA, USA, 2022; pp. 35–124. [[CrossRef](#)]
26. Andre, J.; Siarry, P.; Dognon, T. An improvement of the standard genetic algorithm fighting premature convergence in continuous optimization. *Adv. Eng. Softw.* **2001**, *32*, 49–60. [[CrossRef](#)]
27. Schaffer, J.D.; Eshelman, L.J.; Offutt, D. Spurious Correlations and Premature Convergence in Genetic Algorithms. In *Foundations of Genetic Algorithms*; Rawlins, G.J.E., Ed.; Elsevier: Amsterdam, The Netherlands, 1991; Volume 1, pp. 102–112.
28. Eldeeb, M.A.; Akih-Kumgeh, B. Reactivity Trends in Furan and Alkyl Furan Combustion. *Energy Fuels* **2014**, *28*, 6618–6626. [[CrossRef](#)]
29. Xu, N.; Tang, C.; Meng, X.; Fan, X.; Tian, Z.; Huang, Z. Experimental and Kinetic Study on the Ignition Delay Times of 2,5-Dimethylfuran and the Comparison to 2-Methylfuran and Furan. *Energy Fuels* **2015**, *29*, 5372–5381. [[CrossRef](#)]
30. Li, S.; Huang, C.; Yang, C.; Yu, W.; Liu, J.; Zhang, T. A Reduced Reaction Mechanism for Diesel/2-Methyltetrahydrofuran Dual-Fuel Engine Application. *Energies* **2022**, *15*, 7677. [[CrossRef](#)]
31. Wang, S.; Liang, Y.; Zhu, J.; Raza, M.; Li, J.; Yu, L.; Qian, Y.; Lu, X. Experimental and modeling study of the autoignition for diesel and n-alcohol blends from ethanol to n-pentanol in shock tube and rapid compression machine. *Combust. Flame* **2021**, *227*, 296–308. [[CrossRef](#)]
32. Zhou, W.; Liang, Y.; Pei, X.; Zhang, Y.; Yu, L.; Lu, X. Autoignition of methyl palmitate in low to intermediate temperature: Experiments in rapid compression machine and kinetic modeling. *Combust. Flame* **2023**, *249*, 112619. [[CrossRef](#)]
33. Xu, N.; Wu, Y.; Tang, C.; Zhang, P.; He, X.; Wang, Z.; Huang, Z. Experimental study of 2,5-dimethylfuran and 2-methylfuran in a rapid compression machine: Comparison of the ignition delay times and reactivity at low to intermediate temperature. *Combust. Flame* **2016**, *168*, 216–227. [[CrossRef](#)]

34. Togbé, C.; Tran, L.-S.; Liu, D.; Felsmann, D.; Oßwald, P.; Glaude, P.-A.; Sirjean, B.; Fournet, R.; Battin-Leclerc, F.; Kohse-Höinghaus, K. Combustion chemistry and flame structure of furan group biofuels using molecular-beam mass spectrometry and gas chromatography—Part III: 2,5-Dimethylfuran. *Combust. Flame* **2014**, *161*, 780–797. [[CrossRef](#)]
35. Ma, X.; Jiang, C.; Xu, H.; Shuai, S.; Ding, H. Laminar Burning Characteristics of 2-Methylfuran Compared with 2,5-Dimethylfuran and Isooctane. *Energy Fuels* **2013**, *27*, 6212–6221. [[CrossRef](#)]
36. Wu, X.; Huang, Z.; Wang, X.; Jin, C.; Tang, C.; Wei, L.; Law, C.K. Laminar burning velocities and flame instabilities of 2,5-dimethylfuran–air mixtures at elevated pressures. *Combust. Flame* **2011**, *158*, 539–546. [[CrossRef](#)]
37. Konnov, A.A.; Mohammad, A.; Kishore, V.R.; Kim, N.I.; Prathap, C.; Kumar, S. A comprehensive review of measurements and data analysis of laminar burning velocities for various fuel+air mixtures. *Prog. Energy Combust. Sci.* **2018**, *68*, 197–267. [[CrossRef](#)]

Disclaimer/Publisher’s Note: The statements, opinions and data contained in all publications are solely those of the individual author(s) and contributor(s) and not of MDPI and/or the editor(s). MDPI and/or the editor(s) disclaim responsibility for any injury to people or property resulting from any ideas, methods, instructions or products referred to in the content.